Design and calibration of a wireless laser-based optical sensor for crack propagation monitoring

S.H. Man[*1], C.C. Chang[1a], M. Hassan[2b] and A. Bermak[2c]

[1]*Department of Civil and Environmental Engineering, Hong Kong University of Science and Technology, Clear Way Bay, Kowloon, Hong Kong*
[2]*Department of Electronic and Computer Engineering, Hong Kong University of Science and Technology, Clear Way Bay, Kowloon, Hong Kong*

Abstract. In this study, a wireless crack sensor is developed for monitoring cracks propagating in two dimensions. This sensor is developed by incorporating a laser-based optical navigation sensor board (ADNS-9500) into a smart wireless platform (Imote2). To measure crack propagation, the Imote2 sends a signal to the ADNS-9500 to collect a sequence of images reflected from the concrete surface. These acquired images can be processed in the ADNS-9500 directly (the navigation mode) or sent to Imote2 for processing (the frame capture mode). The computed crack displacement can then be transmitted wirelessly to a base station. The design and the construction of this sensor are reported herein followed by some calibration tests on one prototype sensor. Test results show that the sensor can provide sub-millimeter accuracy under sinusoidal and step movement. Also, the two modes of operation offer complementary performance as the navigation mode is more accurate in tracking large amplitude and fast crack movement while the frame capture mode is more accurate for small and slow crack movement. These results illustrate the feasibility of developing such a crack sensor as well as point out directions of further research before its actual implementation.

Keywords: crack monitoring; optical flow; opticalnavigation

1. Introduction

Occurrence of cracks in concrete structures is not only an issue affecting their appearance but also is a good indication of their deterioration. Excessively wide and deep crack can lead to corrosion of rebars and inevitably affect the durability of these structures. The British Standards BS8110 (1997) states that cracks appear in reinforced concrete structures should be kept within 0.3mm for the purpose of aesthetics and corrosion control. Considering loss of performance such as water tightness, the British Standard BS8007 (1987) further limits the crack width to be 0.1 or 0.2 mm, depending on the allowable stresses of the rebar. Hence, monitoring the changes in crack

∗Corresponding author, Ph.D. Student, E-mail: cemshab@ust.hk
[a] Professor, E-mail: cechang@ust.hk
[b] Ph.D. Student, E-mail: mhassan@ust.hk
[c] Professor, E-mail: eebermak@ust.hk

width is an important diagnostic measure for determining the cause and specifying possible remedial action for important concrete structures.

Currently, there are a few sensors such as the linear variable differential transformer (LVDT), the eddy current sensor and the string potentiometer that can be used for crack monitoring (Kotowsky 2010). An LVDT relies on electromagnetic coupling and converts a linear displacement or position from a mechanical reference into a proportional electrical signal (Measurement Specialties 2013). The eddy current sensor passes an AC current to the sensor coil to produce an oscillating electromagnetic field. Placing the coil at a nominal distance from an electrically conductive target induces an eddy current flow on the surface and within the target. This eddy current produces a secondary magnetic field that opposes and reduces the intensity of the original field, thus creating a coupling effect. This coupling is hence converted by the sensor electronics into a voltage signal proportional to the gap distance (Lion Precision 2013). A string potentiometer is a transducer used to detect and measure linear position and velocity using a flexible cable and spring-loaded spool. Inside the transducer's housing, a stainless steel cable is wound on a cylindrical spool that turns as the measuring cable reels and unreels. The extension of the transducer's cable causes the spool and sensor shafts to rotate and creates an electrical signal proportional to the cable's linear extension or velocity (National Instruments 2013).

Despite the fact that the above-mentioned sensors can be used for long-term crack monitoring, these sensors however have some problems which might limit their implementation on large-scale civil structures. Firstly, these sensors can only measure cracks propagating along the direction aligned with the sensor arrangement, while cracks can propagate in two or even three directions. Secondly, most of these sensors are wired to data loggers and the cabling can be time and labor consuming. Thirdly, stringent installation procedures are usually required for these sensors in order to attain their intended accuracy. Finally, the costs of these sensors are rather high and might prohibit their mass deployment in large-scale civil structures (Kotowsky 2010). These issues suggest the need for developing a crack sensor which can monitor cracks propagating in multiple directions as well as can wirelessly transmit their measured results.

An optical navigation technique refers to the determination of the position and orientation of an object through the analysis of its image sequences. The technique has found its applications in various disciplines including robotic engineering (Hyun *et al.* 2009), autonomous navigation for spacecrafts (Shang and Palamer 2010) and optical mouse for personal computers (Avago Technologies 2013a). Sensors that integrate an illumination source, a camera and a digital signal processor (DSP) have also been developed to facilitate the application of such a technique. The sensors illuminate the surface underneath, acquire the microscopic images of the surface and process these images using pre-loaded program in the DSP. The acquired images can also be output to an external micro-controller for further processing if necessary. Due to a rapid advancement of micro- and nano-fabrication, these optical navigation sensors have been developed not only with better and more versatile specifications to meet different application requirements but also in a more compact size and a lower cost.

In this study, a wireless crack sensor is developed for monitoring cracks that can possibly propagate in two dimensions. This sensor is developed by incorporating a laser-based optical navigation sensor board (ADNS-9500) into a smart wireless platform (Imote2). The design and the construction of this sensor are reported herein followed by some calibration tests on one prototype sensor developed in our laboratory.

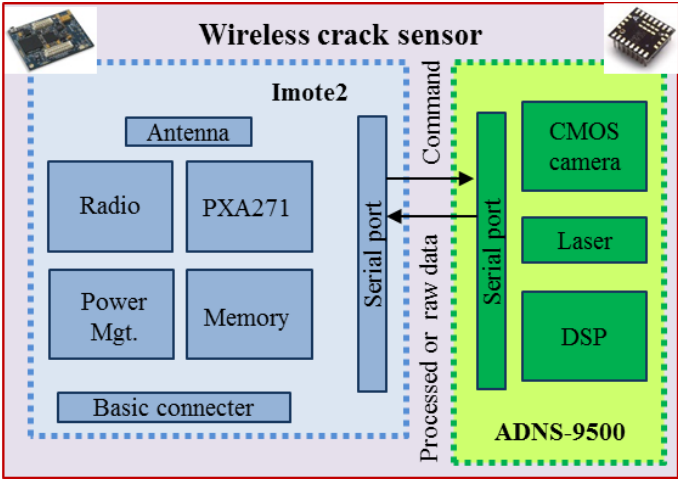## 2. The proposed two-dimensional wireless crack sensor

As mentioned above, the proposed wireless crack sensor consists of a wireless sensor node platform and an optical navigation sensor board. In this paper, the Imote2 board produced by the Crossbow Technology (2013) is adopted as the wireless sensor node platform and the ADNS-9500 produced by the Avago Technologies (2013b) is selected as the optical navigation sensor board. Details about the Imote2 and ADNS-9500 are described below.

The Imote2 board has a compact size of 36 mm x 48 mm x 9 mm. It is built with a 2.4 GHz antenna which can achieve a typical transmission range of 30m (Cho et al. 2010, Jang et al. 2010, Rice *et al.* 2010, Sim *et al.* 2010). The Imote2 also includes an IEEE802.15.4 compliant radio to receive signal from other devices. A battery board is designed to power the Imote2 using three primary AAA batteries. The Imote2 is built around Intel's X scale processor PXA271 for applications requiring intensive computation and high performance. The PXA271 processor can be configured to operate in different modes such as sleep or deep sleep which can enable very low power consumption. The Imote2 contains 256 KB of static random-access memory (SRAM), 32 MB of synchronous dynamic random access memory (SDRAM) and 32 MB of flash memory. The Imote2 also contains an inter-integrated circuit bus (I^2C) and a serial peripheral interface bus (SPI) in order to interface external devices serially. These specifications make the Imote2 very flexible in interacting with different sensors.
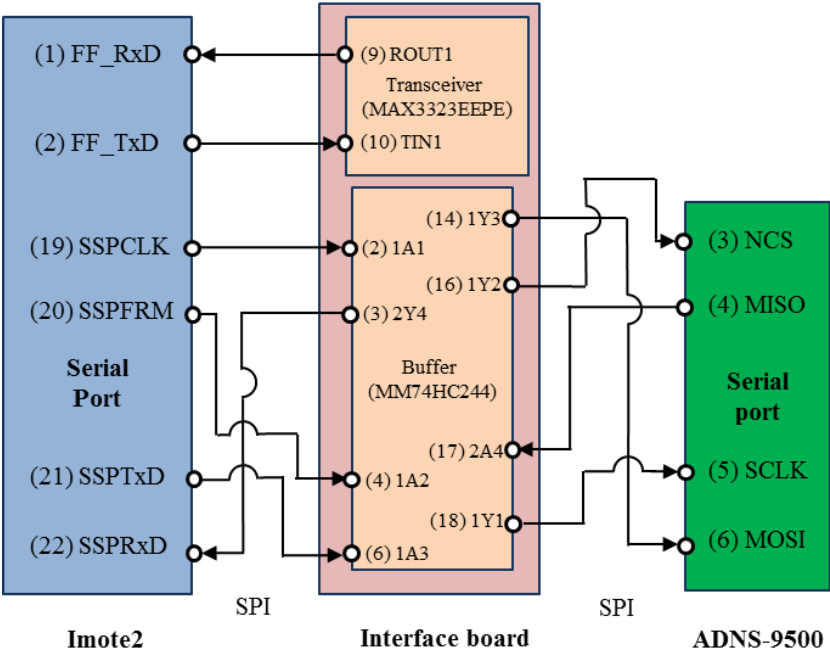
The ADNS-9500 is a high performance optical navigation sensor board that contains a complementary metal-oxide semiconductor (CMOS) camera and an 832-865nm wavelength vertical-cavity surface-emitting laser (VCSEL) in a single chip-on-board package (Avago Technologies 2013b). The sensor board contains an image acquisition system (IAS), a built-in DSP and a four-wire serial port. The IAS acquires microscopic images of surface illuminated by the VCSEL. The captured image has a resolution of 30×30 pixels. Each pixel has 7 bits values. There are two modes of operation for the ADNS-9500: the navigation mode and the frame capture mode. In the navigation mode, the images are processed by the built-in DSP to determine the direction and distance of movement between the ADNS-9500 and the surface. The sensitivity of the movement can be up to 5,000 counts per inch (CPI) with a step increment of 90 CPI. In the frame capture mode, the ADNS-9500 outputs a full array of pixel values of a captured image via the serial port. The ADNS-9500 can be switched from one mode to another through an external command.

In our proposed design, the ADNS-9500 board is interfaced with the Imote2 board via the serial port as shown in Fig. 1(a). The 4 pins of the serial port on the Imote2 board are connected to the corresponding 4 pins of the serial port on the ADNS-9500 through an interface board as shown in Fig. 1(b). Note that the number inside the brackets denote the pin numbers shown in the datasheets of the Imote2 (Crossbow Technology 2013) and the ADNS-9500 (Avago Technologies 2013b).The interface board contains a non-inverting buffer MM74HC244 (Fairchild Semiconductor 2014)and a transceiverMAX3323EEPE (Maxim Integrated Products 2014). The MM74HC244 buffer is a general purpose high speed non-inverting 3-state buffer utilizing advanced silicon-gate CMOS technology. This buffer has a capability to drive high current at output and hence can achieve high speed operation. Furthermore, the built-in hysteresis on each input data line of the buffer greatly helps to improve noise margin and offer high fan-out outputs to prevent the ADNS-9500 from unexpectedly loading and interfering with the Imote2. The MAX3323EEPE transceiver on the other hand is a communication interface designed for multi drop applications with low power

requirements to provide an option for the Imote2 to connect to other sensors in parallel with ADNS-9500when needed.

(a)

(b)

Fig. 1 Proposed crack sensor: (a) schematic diagram (b) electronic design

Fig. 2 shows a functional flowchart for the proposed wireless crack sensor. The PXA271 processor on the Imote2 board acts as the "brain" of the wireless crack sensor and communicates with the ADNS-9500. For crack monitoring, the PXA271 sends a command signal to the ADNS-9500 sensor to turn on the VCSEL and the CMOS camera to collect images reflected from the concrete surface. Depending on the command from the PXA271, the ADNS-9500 will operate in either (1) the navigation mode: process the captured images in its built-in DSP and pass the computed movement of the concrete surface to the PXA271 or (2) the frame capture mode: send the captured raw images to the Imote2 to compute movement between the images through an algorithm such as the optical flow technique residing in the PXA271. Note that the movement obtained from the navigation mode and the frame capture mode are in terms of counts and pixels respectively in the image domain.

To obtain the displacement in the physical domain, it is necessary to calibrate the sensor and obtain scale factors between the image and the physical domain. The conversion can again be done in the Imote2. The obtained displacements can then be sent wirelessly to a base station for further processing or for diagnosing. Note that the frequency of image acquisition in the frame capture mode can be set by the PXA271 which in turns can be accessed and controlled wirelessly by the base station.

For installation, the wireless crack sensor needs to be positioned across the crack with one end glued to the concrete surface and the other end in contact with the concrete surface via a low-friction rubber pad. Figure 3 shows the top view and the side view for the sensor installation. The glued edge of the sensor and the ADNS-9500 should be split between the two sides of crack. As the crack width changes concrete surface underneath the ADNS-9500 will move relative to the sensor and such relative movements can be determined using either the navigation mode or the frame capture mode.

3. The optical flow technique

As the propagation of crack is usually in the order of micro-meter (Dowding and McKenna 2005), it is essential to incorporate an accurate motion estimation into the Imote2 board. This motion estimation algorithm preferably should have a low computational requirement to minimize the energy consumption for wireless sensing application. In this study, an optical flow method which can provide real-time estimation with sub-pixel accuracy is adopted (Ji and Chang 2008, Ciliberto *et al.* 2011). As shown in Fig. 4, the optical flow technique can be used to determine the movements in the image coordinates Δu and Δv (along the image coordinates u and v, respectively) between the reference image recorded at time t and the subsequent image recorded at $t+\Delta t$. Assume that the intensity value of an arbitrary point $j_i(u,v,t)$ in the reference image is expressed as $I_i(u,v,t)$, where $i=1,2,...n^2$ is an index of pixels inside the region of interest (ROI).The intensity value is defined as the intensity of light sensed by the camera at each pixel. For the camera residing in the ADNS-9500, it comes with a 7-bit resolution and gives intensity values ranging between 0 and 127. In the subsequent image, this point $I_i(u,v,t)$ moves to $j_i(u+\Delta u,v+\Delta v,t+\Delta t)$ which intensity value is denoted as $I_i(u+\Delta u,v+\Delta v,t+\Delta t)$. Assume the two intensity values remain the same before and after the movement (Lucas and Kanade 1981)
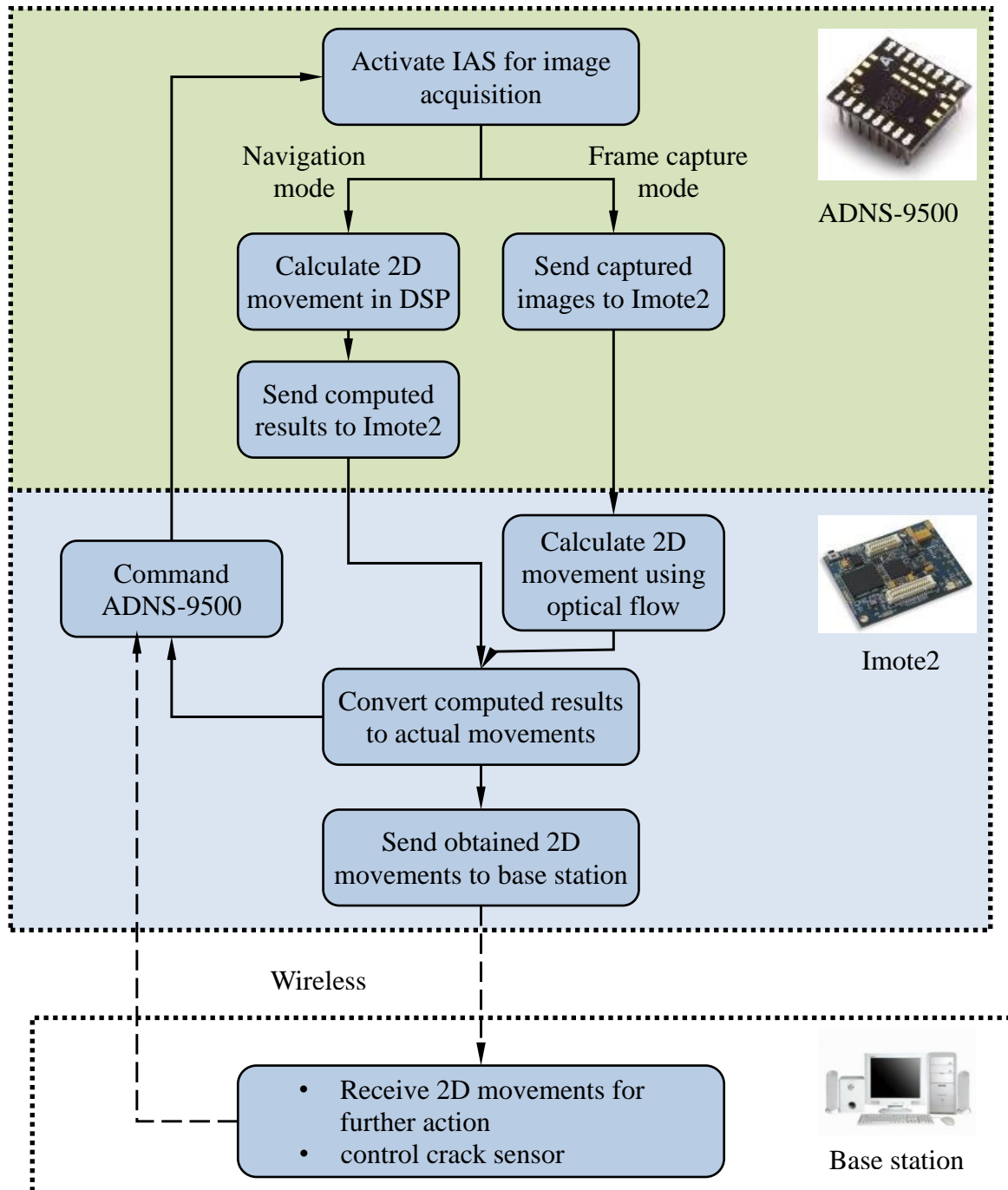
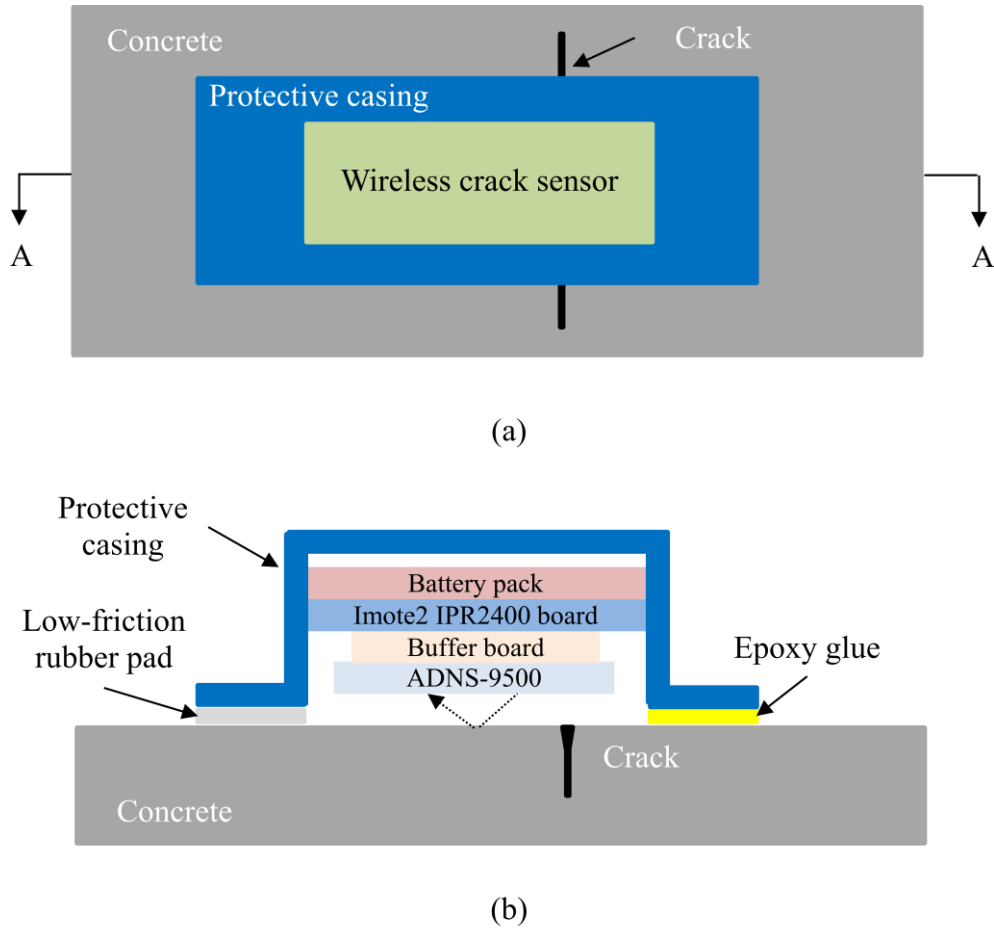Fig. 2 Functional flowchart of the proposed crack sensor

(a)

(b)

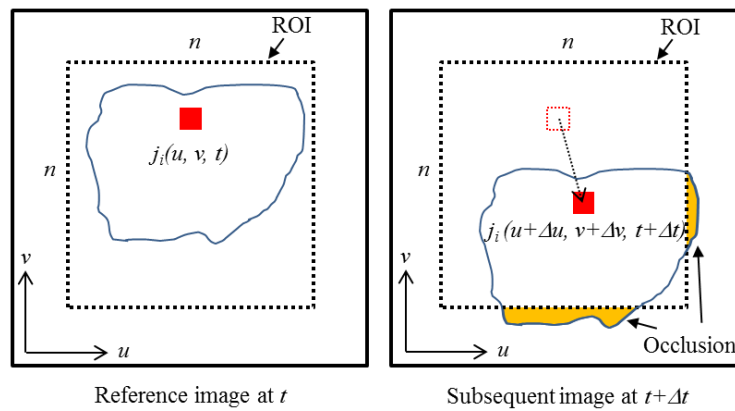Fig. 3 Sensor installation: (a) top view and (b) side view of section A-A

Fig. 4 Motion estimation by the optical flow method

$$I_i(u,v,t) = I_i(u + \Delta u, v + \Delta v, t + \Delta t) \tag{1}$$

Expanding the right-hand side of Eq. (1) by a Taylor series expansion and retaining the 0th and the 1st order terms give

$$I_i(u + \Delta u, v + \Delta v, t + \Delta t) = I_i(u,v,t) + I_{i,u}\Delta u + I_{i,v}\Delta v + I_{i,t}\Delta t \tag{2}$$

where $I_{i,u}, I_{i,v}$, and $I_{i,t}$ denote the partial derivatives of the intensity of a particular pixel I_i with respect to u, v, and t, respectively. These three intensity derivatives can be obtained from the first-order finite difference analysis between the reference image and the subsequent image. Combing Eqs. (1) and (2) leads to the following optical flow constraint

$$I_{i,u}\Delta u + I_{i,v}\Delta v = -I_{i,t}\Delta t \tag{3}$$

Note that the information from one pixel is not sufficient to determine the movements Δu and Δv (Jain *et al.* 1995). To overcome this problem, a region of interest (ROI) of $n \times n$ pixels is selected and all pixels inside this ROI are assumed to have the same Δu and Δv. Expressing Eq. (3) for all pixels inside the ROI leads to

$$\begin{bmatrix} I_{1,u} & I_{1,v} \\ I_{2,u} & I_{2,v} \\ \vdots & \vdots \\ I_{n^2,u} & I_{n^2,v} \end{bmatrix} \begin{Bmatrix} \Delta u \\ \Delta v \end{Bmatrix} = - \begin{Bmatrix} I_{1,t} \\ I_{2,t} \\ \vdots \\ I_{n^2,t} \end{Bmatrix} \Delta t \tag{4}$$

To obtain Δu and Δv, a least square optimization is performed which leads to

$$\begin{bmatrix} \sum_{i=1}^{n^2} I_{i,u} I_{i,u} & \sum_{i=1}^{n^2} I_{i,u} I_{i,v} \\ \sum_{i=1}^{n^2} I_{i,u} I_{i,v} & \sum_{i=1}^{n^2} I_{i,v} I_{i,v} \end{bmatrix} \begin{Bmatrix} \Delta u \\ \Delta v \end{Bmatrix} = - \begin{Bmatrix} \sum_{i=1}^{n^2} I_{i,u} I_{i,t} \\ \sum_{i=1}^{n^2} I_{i,v} I_{i,t} \end{Bmatrix} \Delta t \tag{5}$$

Hence

$$\Delta u = \frac{\sum\limits_{i=1}^{n^2} I_{i,u} I_{i,v} \sum\limits_{i=1}^{n^2} I_{i,v} I_{i,t} - \sum\limits_{i=1}^{n^2} I_{i,v} I_{i,v} \sum\limits_{i=1}^{n^2} I_{i,u} I_{i,t}}{\sum\limits_{i=1}^{n^2} I_{i,u} I_{i,u} \sum\limits_{i=1}^{n^2} I_{i,v} I_{i,v} - \left(\sum\limits_{i=1}^{n^2} I_{i,u} I_{i,v} \right)^2} \Delta t \tag{6}$$
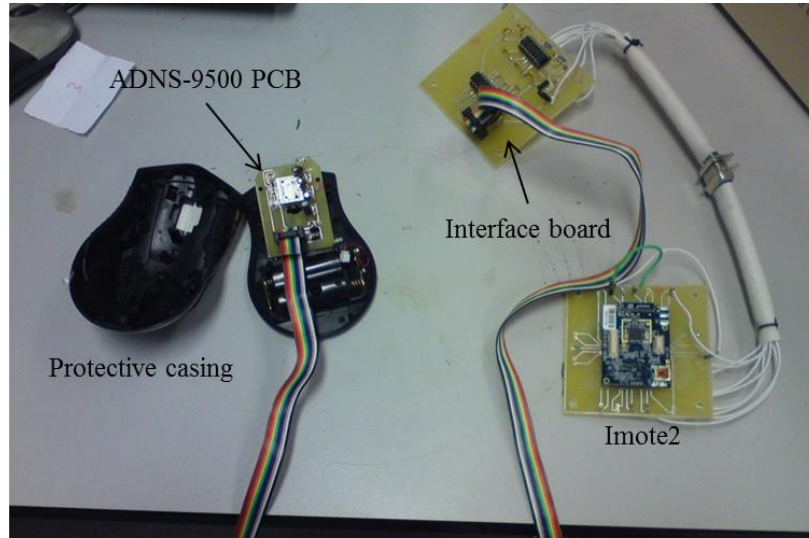
$$\Delta v = \frac{\sum_{i=1}^{n^2} I_{i,u} I_{i,v} \sum_{i=1}^{n^2} I_{i,u} I_{i,t} - \sum_{i=1}^{n^2} I_{i,u} I_{i,u} \sum_{i=1}^{n^2} I_{i,v} I_{i,t}}{\sum_{i=1}^{n^2} I_{i,u} I_{i,u} \sum_{i=1}^{n^2} I_{i,v} I_{i,v} - \left(\sum_{i=1}^{n^2} I_{i,u} I_{i,v}\right)^2} \Delta t \tag{7}$$

It can be seen from Eqs. (6) and (7) that Δu and Δv depend on the selection of ROI. The relationship between measurement accuracy and the size of ROI will be discussed in the latter session. Note that Δu and Δv are obtained in pixel values. To obtain the actual displacement increments, it is necessary to know the physical dimensions of the pixel which can be obtained through a calibration test. Details of this test will also be reported in the following session.
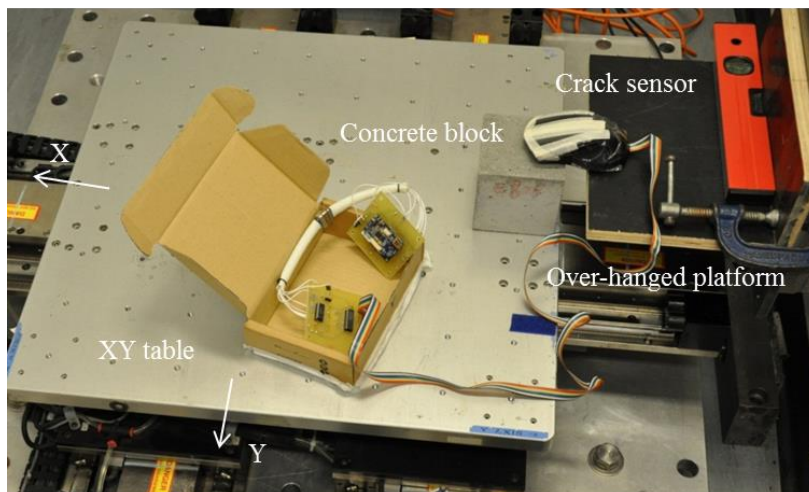
Since the above optical flow technique is formulated based on a Taylor series expansion, errors in the estimation of movements are unavoidable. It is expected that the errors would be larger for a larger movement (or equivalently faster crack propagation). Also, the location of the ROI is assumed to be the same on both images as shown in Fig. 4. This means that some of the feature in the ROI of the reference image would be occluded from the ROI in the subsequent image. Again, a larger movement or fast crack propagation would increase the occluded area and leads to a larger estimation error. In summary, the accuracy of the optical flow technique adopted above would be more accurate for small movements.

4. Calibration and performance tests

A prototype crack sensor was fabricated in the laboratory and is shown in Fig. 5(a). The ADNS-9500 board was wire-connected to the Imote2 board via a interface board. The ADNS-9500 board was placed inside a computer mouse casing which was used to protect the board during the tests. A software responsible for the communication between the Imote2 and the ADNS-9500 together with the optical flow technique reported above were programmed under C# . NET Micro framework and resided in the Imote2. Depending on the mode of operation, the acquired images were processed either at the ADNS-9500 board (navigation mode) or at the Imote2 board (frame capture mode). The power consumption for the prototype crack sensor was about 850 mW disregard whether it is operated in the navigation mode or the frame capture mode. The processed data were then transmitted wirelessly to an external computer via the Imote2 board. A series of experimental tests were conducted to calibrate as well as to study the accuracy of the proposed crack sensor. These tests were performed on a shake table which could be programmed to move in two directions respectively or simultaneously. The ADNS-9500 board was mounted on a fixed over-hanged platform on one side and the VCSEL and the CMOS camera were placed on top of a concrete block which was fixed on the shake table. The movement of the shake table with the concrete block was to simulate the actual crack opening and was measured by the sensor. Fig. 5(b) shows the experimental setup for the proposed crack sensor. Fig. 6 shows a typical image captured from the ADNS-9500. It is seen that there is a bright yet random region in the middle of both images which can be referred to as a laser speckle pattern (Goodman and Parry 1984, Liao *et al.* 2009). The pattern is a result of a coherent laser light scattering off a rough surface.

(a)

(b)

Fig. 5(a) Prototype and (b) experimental setup for the prototype crack sensor

4.1 Sensor calibration

The prototype crack sensor needs to be calibrated to establish the dimensional relationship between the image domain and the physical domain. The shake table was first programmed to move at a constant speed along the 45° direction (see Fig. 5) for a fixed distance of 1, 2 ... and 10 mm, respectively. Eleven different speeds were selected: 0.01, 0.05, 0.1, 0.15, 0.2 ... and 0.5 mm/s. The acquired images were processed through both the navigation mode and the frame capture mode.

Fig. 6 A typical image captured by the ADNS 9500 from the concrete surface

Fig. 7(a) shows the output along the X direction and Y direction, respectively, obtained from the navigation mode plotted against the displacement of the shake table along the X direction and Y direction, respectively, under the speed of 0.01, 0.2, 0.3 and 0.5 mm/s, respectively. The sampling frequency of the crack sensor was set at 15 Hz. In the navigation mode, the acquired images were directly processed in the ADNS-9500 and the computed results were sent to the Imote2 board before wirelessly transmitted to a computer. The unit of output did not carry any physical meaning prior to the calibration and was simply termed as "count" on the figure. It is seen that the output are linear to the table displacement but differ quite distinctly under different shake table speeds. This indicates that the output from the navigation mode is affected by the speed of movement.

To further investigate the effect of speed on the performance of the crack sensor under the navigation mode, the sensitivity of the sensor (count/mm) is plotted against the speed of movement in Fig. 7(b). It is seen that the sensitivity of the sensor is significantly affected by the speed of movement especially when the speed of movement is below 0.1 mm/s. Note also that the sensitivity seems to saturate at 92 count/mm when the speed of movement is higher than 0.4 mm/s.

To see whether the sampling frequency would affect the sensor's sensitivity, the experiments were repeated using two different sampling frequencies: 5 Hz and 10 Hz. The results from the navigation mode were obtained and again plotted in Fig. 7(b). It is seen that the sensitivity of sensor is not affected significantly by the sampling frequency. To further examine this observation, zoomed plots of Fig. 7(b) are provided in Fig. 7(c). This suggests that the insensitivity and the lack of robust performance of the navigation mode at the low speed region cannot be improved by the change of sampling frequency. These results reveal that the navigation mode is more suitable when the speed of movement is larger than 0.4 mm/s.

Next, the sensor was switched to operate in the frame capture mode. In this mode, the PXA271 processor on the Imote2 board acquires images from the ADNS-9500. These images are then processed through the optical flow technique in the processor. The size of ROI *n* was chosen to be 30 and the sampling frequency was set at 15 Hz. Fig. 8(a) shows the output along the X direction and Y direction, respectively, obtained from the frame capture mode plotted against the displacement of the shake table along the X direction and Y direction, respectively, under the speed of 0.01, 0.2, 0.3 and 0.5 mm/s. It is seen that the computed displacements along the X

direction under the speed of 0.01, 0.2 and 0.3 mm/s are almost identical while those obtained under the speed of 0.5 mm/s are lower in comparison.
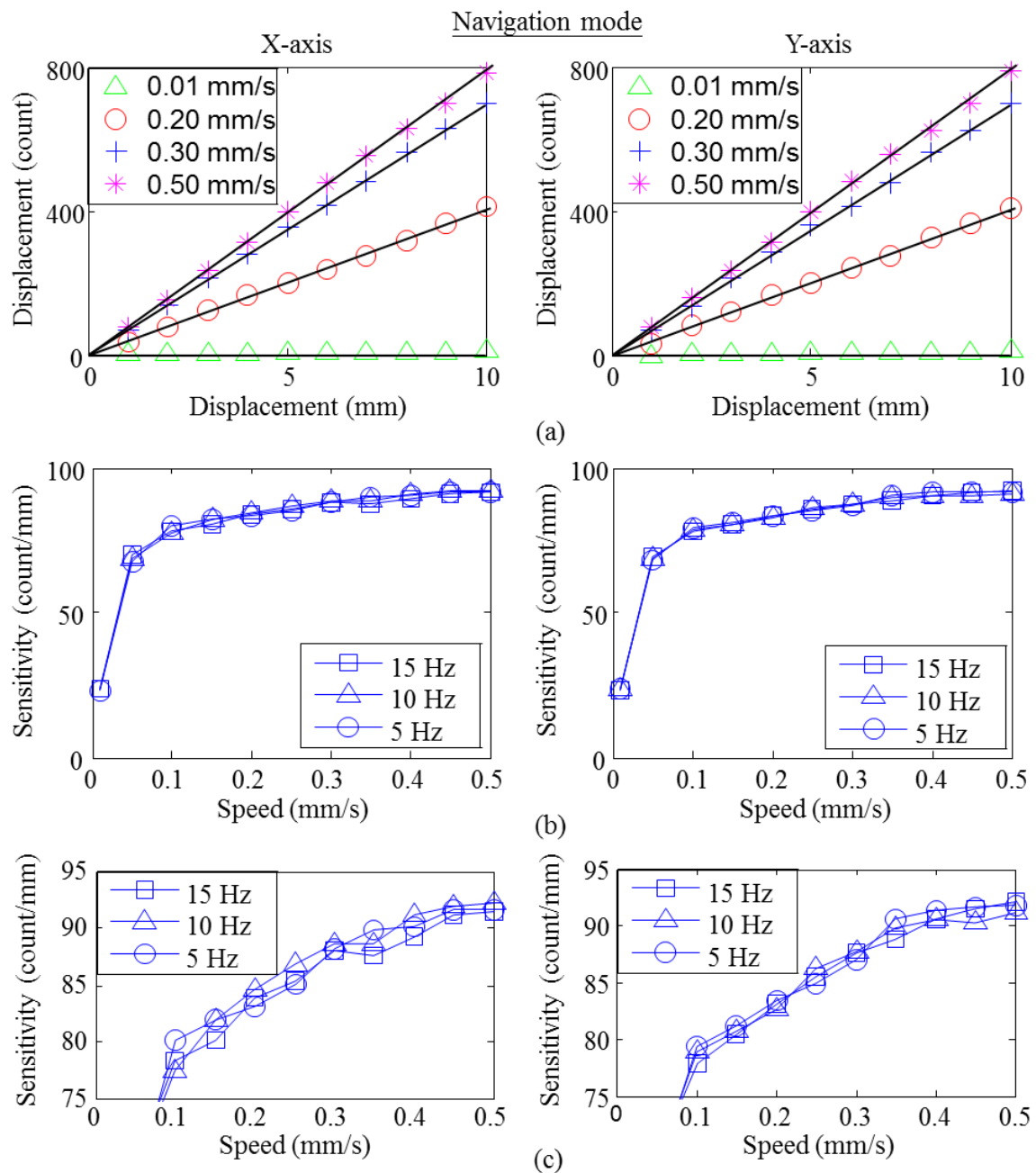

Fig. 7 (a) Calibration curves with f = 15 Hz; (b) sensitivity-speed relationship using navigation mode; and (c) zoomed plot of Fig. 7(b)

The effect of speed on the performance of the crack sensor under the frame capture mode was further investigated by plotting the sensitivity of sensor (pixel/mm) against the speed of movement in Fig. 8(b). It is seen that the sensitivity of the sensor under the sampling frequency of 15 Hz is rather constant at the value of 20 pixel/mm for the speed of movement up to 0.4 mm/s. The sensitivity of sensor however decreases as the speed further increases. To see whether the sampling frequency would affect the sensor's sensitivity, the experiments were repeated using two different sampling frequencies: 5 Hz and 10 Hz. The results were obtained and again plotted in Fig. 8(b). It is seen that the sensitivity of sensor is not affected significantly by the sampling frequency when the speed is lower than 0.1 mm/s. As the speed increases, the sensitivity of sensor reduces as the sampling frequency decreases. It can be concluded from these results that the performance of sensor under the frame capture mode is quite robust under low speed movement (below 0.1 mm/s). Unlike the navigation mode, the sampling frequency would affect the sensitivity of sensor under the frame capture mode. A higher sampling frequency can offer a broader range of speed (up to 0.4 mm/s) for a more robust sensitivity (constant at 20 pixel/mm).

Comparing the two sets of results shown in Figs. 7 and 8, it can be seen that the speed range for a robust sensitivity performance of the sensor is quite different between the two modes of operation. While the navigation mode offers a robust sensitivity of 92 count/mm for speed of movement larger than 0.4 mm/s, the frame capture mode is more robust at 20 pixel/mm for speed of movement smaller than 0.1 mm/s. This suggests that it might be necessary to switch between the two modes depending on the speed of movement during the operation in order to have a robust performance for the whole spectrum of speed.
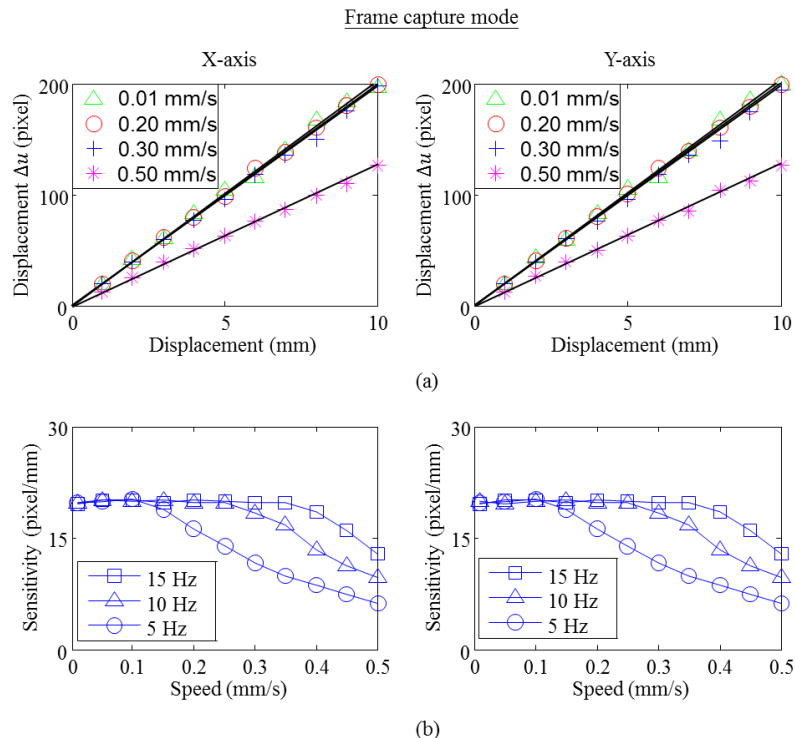

Fig. 8 (a) Calibration curves with f = 15 Hz and (b) sensitivity-speed relationship using frame capture mode
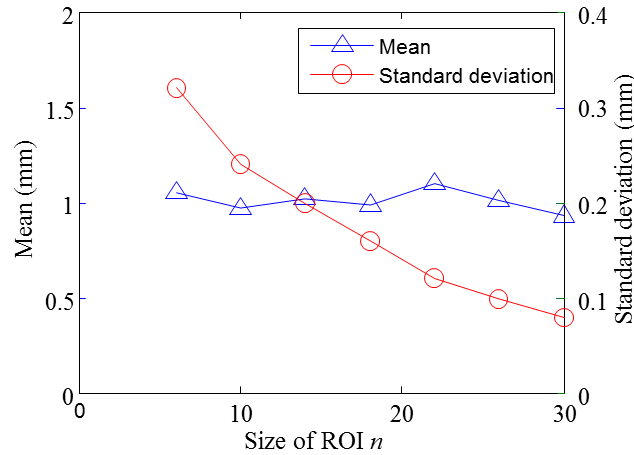
Fig. 9 Performance of the crack sensor under the frame capture mode after moving 1 mm in a constant speed
of 0.2 mm/s: mean and SD against the size of ROI *n*

To study whether the size of ROI *n* would affect the accuracy of measurement under the frame capture mode, seven different size of ROI were used: *n*= 6, 10, 14, 18, 22, 26 and 30 to calculate the movement of the shake table using the optical flow technique. The shake table was programmed to move 1 mm at a constant speed of 0.2 mm/s. The sampling frequency was set at 15 Hz. The test was repeated 10 times to obtain statistical values of the measurement. Fig. 9 shows the means and the standard deviations (SD's) of the measurement. It is seen that the means of the measurement using different sizes of ROI are rather constant at around 1mm. On the other hand, their SD's reduce from about 0.3 mm to about 0.1 mm as *n* increases from 6 to 30. These results show that the size of ROI would affect the measurement noise and a larger ROI would lead to smaller measurement noise.

4.2 Sinusoidal tests

Next, the shake table was programmed to move in a sinusoidal function along the 45° direction (see Fig. 5). Five different peak-to-peak vibration amplitudes (A= 0.1, 0.2, 0.3, 0.5 and 1.0 mm) under five different vibration frequencies (f_v = 0.1, 0.2, 0.3, 0.5 and 1.0 Hz) were tested. For each test, the sensor was operated for 30 seconds. The sensor was first switched to operate in the navigation mode. Fig. 10 shows the results for three cases under a fixed f_v = 0.1 Hz: (1) A= 0.1 mm; (2) A= 0.3 mm; and (3) A=1 mm. It is seen that the sensor operating in the navigation mode cannot track case (1) very well in both X and Y directions. On the other hand, the sensor can measure the sinusoidal motion of case (3) very well. Fig. 11 shows the results for three cases under fixed A = 0.1 mm: (1) f_v = 0.1 Hz; (2) f_v = 0.3 Hz; and (3) f_v =1 Hz. Again it is seen that the sensor operating in the navigation mode cannot track case (1) very well in both X and Y directions. On the other hand, the sensor can measure the sinusoidal motion of case (3) very well. To further investigate the sensor's performance, the means and the SD's of errors between the sensor's output and the prescribed motion for all five vibration amplitudes under five different vibration

frequencies are plotted and shown in Fig. 12. It is seen that the in general both the means and the SD's of measurement errors are smaller as the vibration amplitude increases. Also, under a fixed vibration amplitude, the means and the SD's of measurement errors become smaller as the vibration frequency increases from 0.1 to 1 Hz. These results reveal that the accuracy of sensor under the navigation mode is much better under larger vibration amplitudes and frequencies.
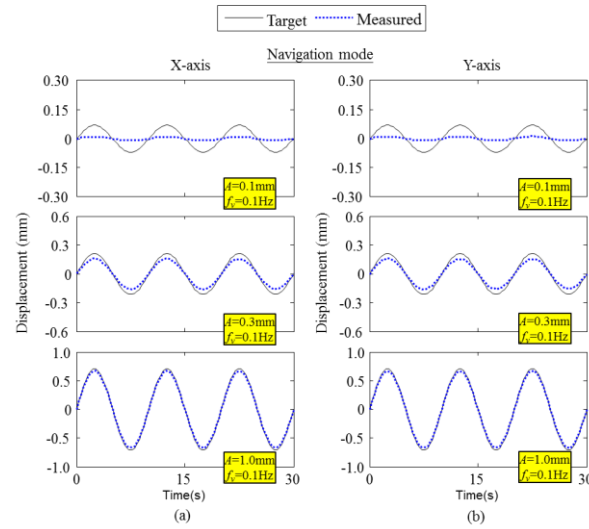

Fig. 10 Performance of the crack sensor for 2D sinusoidal motions using navigation mode under fixed f_v = 0.1 Hz: response along (a) X-axis and (b) Y-axis
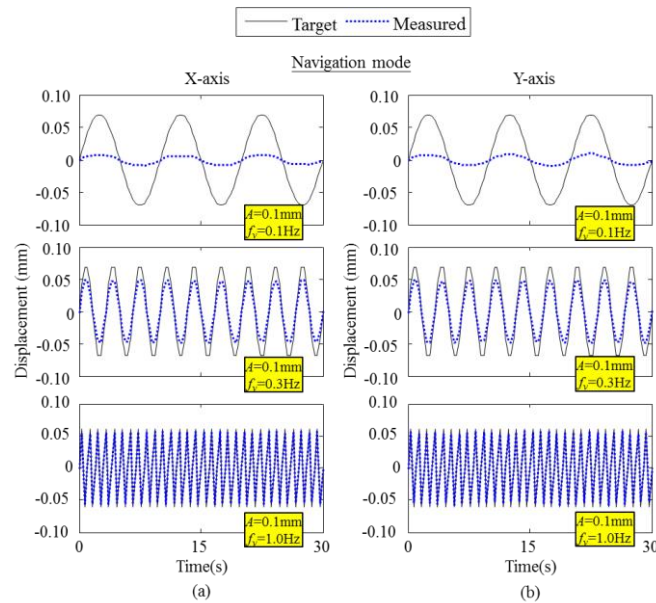

Fig. 11 Performance of the crack sensor for 2D sinusoidal motions using navigation mode under fixed A = 0.1 mm: response along (a) X-axis and (b) Y-axis
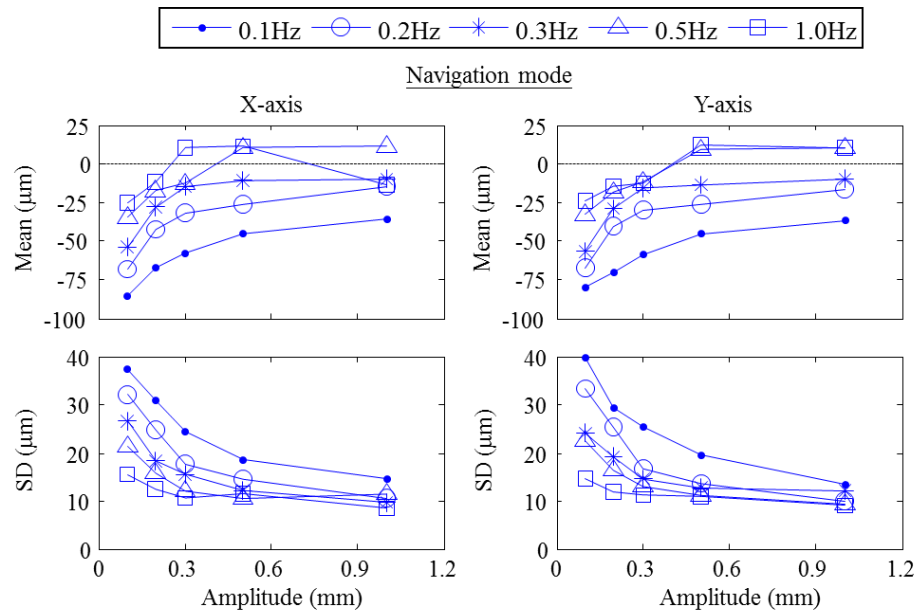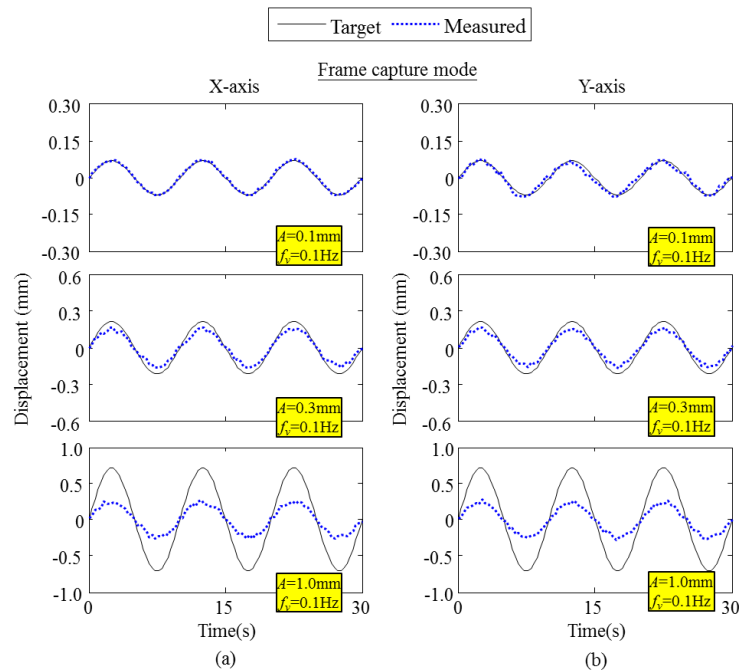
Fig. 12 Means and SDs of measurement errors for 2D sinusoidal motion using navigation mode

Fig. 13 Performance of the crack sensor for 2D sinusoidal motions using frame capture mode under fixed f_v = 0.1 Hz: response along (a) X-axis and (b) Y-axis

For the frame capture mode, the sampling frequency was set at 15 Hz and the size of ROI n was chosen as 30. The same twenty five tests used above were performed. To compare with the results obtained in the navigation mode, the results for the same three cases under a fixed vibration frequency (f_v = 0.1 Hz) and a fixed amplitude (A = 0.1 mm) are obtained and plotted in Figs. 13 and 14, respectively. It is seen that the performance of the frame capture mode is not the same as that of the navigation mode. Under the frame capture mode, the sensor is able to track small amplitude and low frequency better which seems to be just the opposite of when the sensor is operated in the navigation mode. Fig. 15 further shows the means and the SD's of errors between the sensor's output and the prescribed motion for all five vibration amplitudes under five different vibration frequencies. It is seen that both the means and SD's of measurement errors are smaller for small vibration amplitude as well as small vibration frequency. These results conclude that the performance of sensor's frame capture mode is not the same as it's navigation mode. In addition, the two modes of operation seem to complement each other in the sense that the frame capture mode is more accurate under low vibration amplitude and frequency while the navigation mode is more accurate under large vibration amplitude and frequency.
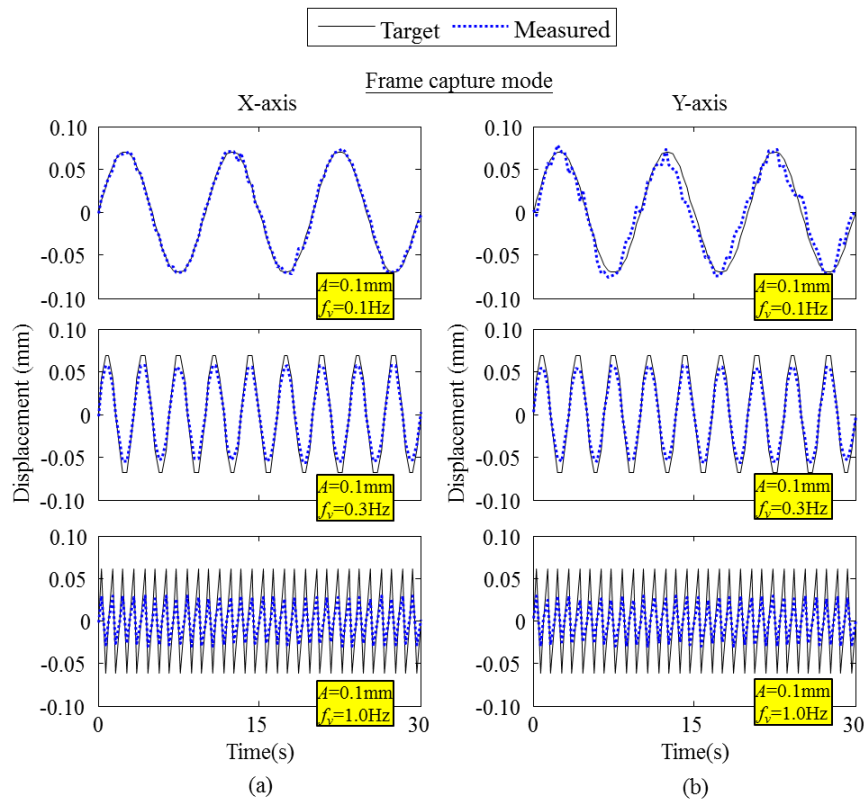

Fig. 14 Performance of the crack sensor for 2D sinusoidal motions using frame capture mode under fixed A = 0.1 mm: response along (a) X-axis and (b) Y-axis

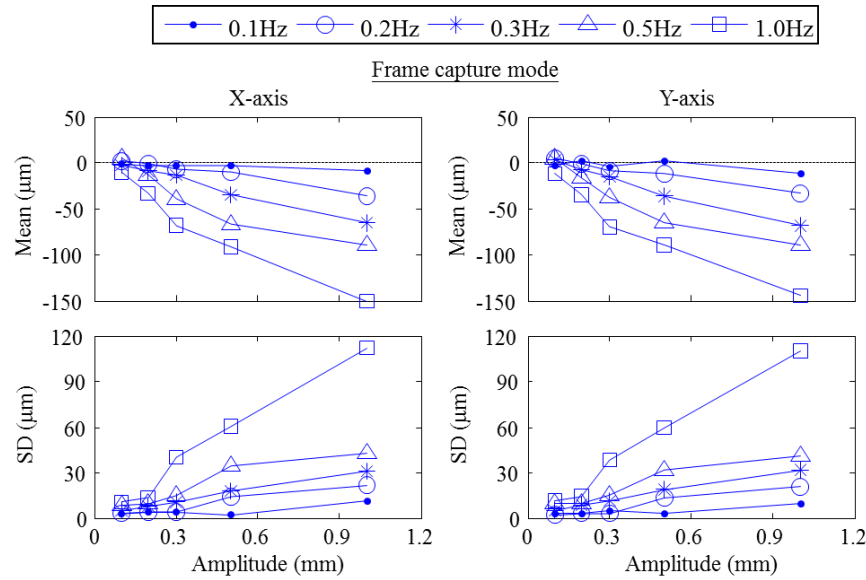*S.H. Man, C.C. Chang, M. Hassan and A. Bermak*

Fig. 15 Means and SDs of measurement errors for 2D sinusoidal motion using frame capture mode
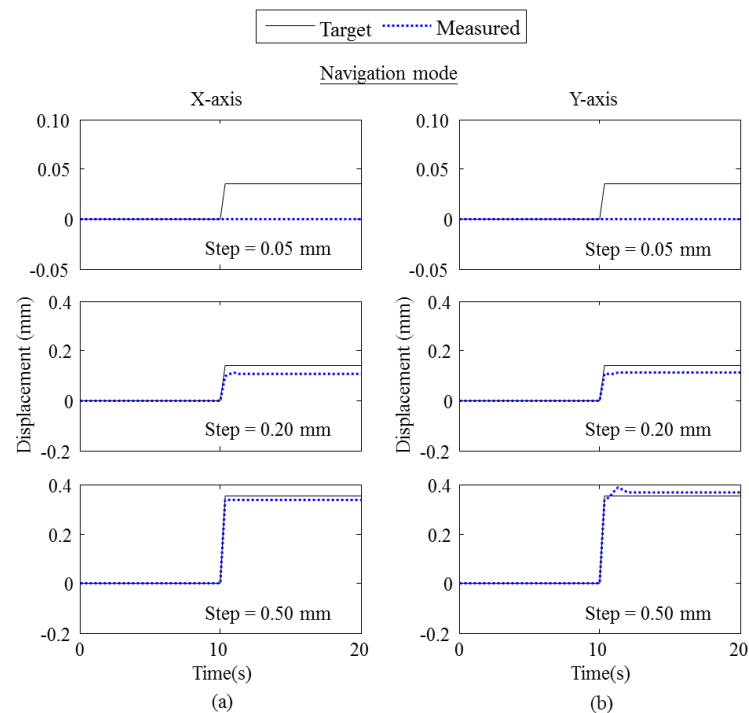

Fig. 16 Performance of crack sensors for 2D step motions using navigation mode: response along (a) X-axis and (b) Y-axis
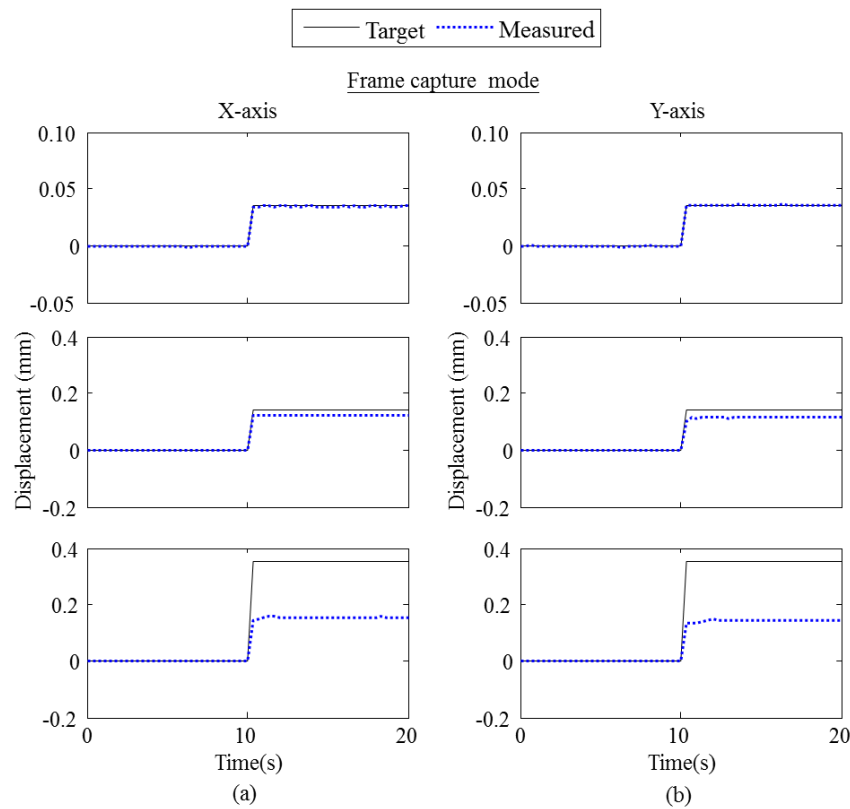
Fig. 17 Performance of crack sensors for 2D step motions using frame capture mode: response along (a) X-axis and (b) Y-axis

4.3 Step tests

In these tests, the shake table was programmed to move with different steps (from 0.05 mm to 0.5 mm) along the 45° direction. Each step movement was completed in 0.3 s. These tests were used to study the performance of sensor under a sudden crack opening. Figure 16 shows the results obtained under the navigation mode for a step movement of 0.05, 0.2 and 0.5 mm, respectively. It is seen that the navigation mode cannot track the small step movement of 0.05 mm at all, while on the other hand the tracking of 0.2 and 0.5 mm is very well. Next the sensor was switched to the frame capture mode and the sampling frequency and the size of ROI n were set at 15 Hz and 30, respectively. The results for a step movement of 0.05, 0.2 and 0.5 mm are shown in Fig. 17. It is seen that the sensor under the frame capture mode performs the best when the step movement is equal to 0.05 mm. The performance deteriorates when the step movement increases. Fig. 18 shows the means the one SD bound of measurement error plotted against the step size for the sensor under the navigation mode and the frame capture mode respectively. Results from the navigation mode reveal that the measurement error is quite significant when the step size is below 0.2 mm. On the other hand, the frame capture mode performs just to the opposite of the navigation mode and is more accurate when the step size is below 0.2 mm.
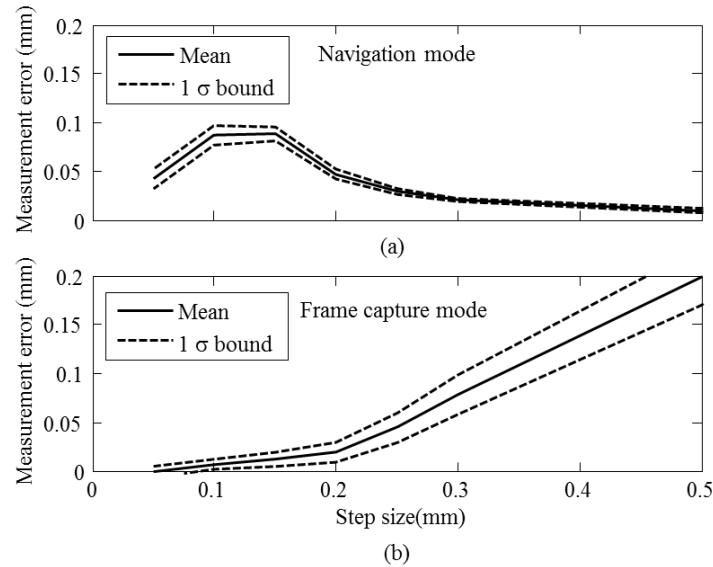
Fig. 18 Measurement errors for 2D step motion under (a) the navigation mode and (b) the frame capture
        mode

5. Discussions

Based on the sinusoidal and step motion tests performed above, it is clear that the sensor operating in the navigation mode can track quite accurately sinusoidal motion of vibration amplitude > 0.3 mm and vibration frequency > 0.3 Hz as well as step motion > 0.2 mm. When switched to the frame capture mode, the sensor can track sinusoidal motion of vibration amplitude < 0.3 mm, vibration frequency < 0.3 Hz and step motion < 0.2 mm. These performance differences might be attributed to the use of different algorithms behind the navigation and the frame capture mode. It appears that the algorithm adopted in the ADNS-9500 is a correlation-based method (Avago 2013a) which relies on bilinear interpolation for the detection of sub-pixel movement. This bilinear interpolation unavoidably introduce errors when the movement between two images is in the sub-pixel range. Furthermore, the small motion calculated from the correlation method in the ADNS-9500 might be filtered to achieve better overall tracking results (Park *et al*. 2007). On the other hand, as can be seen from Eqs. (1) to (3), the optical flow method uses the first two terms from the Taylor series expansion of the image intensities. This implies that the optical flow method would lead to significant errors when the movement between two images becomes large. These results suggest that the two modes of operation, the navigation mode and the frame capture mode, can be used in a complementary fashion to maintain the overall measurement accuracy of the sensor. The sensor should operate in the frame capture mode for small and slow crack movement and be switched to the navigation mode when the crack movement becomes large and fast. Logical calculi for switching between the navigation mode and the frame capture mode are hence proposed based on the sensitivity-speed profiles shown in Figs. 7 and 8. As concluded above, robust performance of the sensor can be obtained when the speed of crack movement is larger than 0.4

mm/s for the navigation mode and smaller than 0.1 mm/s for the frame capture mode, respectively. Hence the middle speed of 0.25 mm/s is chosen as the threshold value for switching between the frame capture and the navigation mode. The frame capture mode is used when the speed of crack movement is smaller than 0.25 mm/s. As the speed increases beyond 0.25 mm/s, the sensor will be switched to the navigation mode. Note that the speed of crack movement can be obtained at each step of calculation by dividing the calculated movement value by the sampling time.

These logical calculi were implemented into the Imote2 and validated by the same sinusoidal tests as shown in Figs. 10, 11, 13 and 14.The sampling frequency of the sensor was set at 15 Hz for all tests. Fig. 19 shows the tracking of f_v= 0.1 Hz sinusoidal motion along 45° direction under three different amplitudes, A= 0.1, 0.3 and 1 mm, respectively. Comparing to the results shown in Fig. 10 (navigation mode) and Fig. 13 (frame capture mode), it is seen that the sensor is able to track the movement of all three cases rather accurately. This shows that the navigation mode and the frame capture mode can be used in a complementary fashion to achieve more robust performance for the sensor. Similarly, the results of fixed amplitude A= 0.1 mm sinusoidal motion under three different frequencies, f_v= 0.1, 0.3 and 1.0 Hz are shown in Fig. 20. Again, comparing to those shown in Fig. 11 (navigation mode) and Fig. 14 (frame capture mode) these results show that the sensor operating in the combined mode is able to track the sinusoidal movement better than its single mode operation. Fig. 21 further shows the means and the SD's of errors between the sensor's output and the prescribed motion for five vibration amplitudes (A= 0.1, 0.2, 0.3, 0.5 and 1 mm) under five different vibration frequencies (f_v= 0.1, 0.2 0.3, 0.5 and 1.0 Hz). Comparing to Fig. 12 (navigation mode) and Fig. 15 (frame capture mode), it is seen that both the means and SD's of measurement errors are smaller for all cases. These results also confirm that more robust performance can be obtained after combining the navigation mode and the frame capture mode into the sensor.
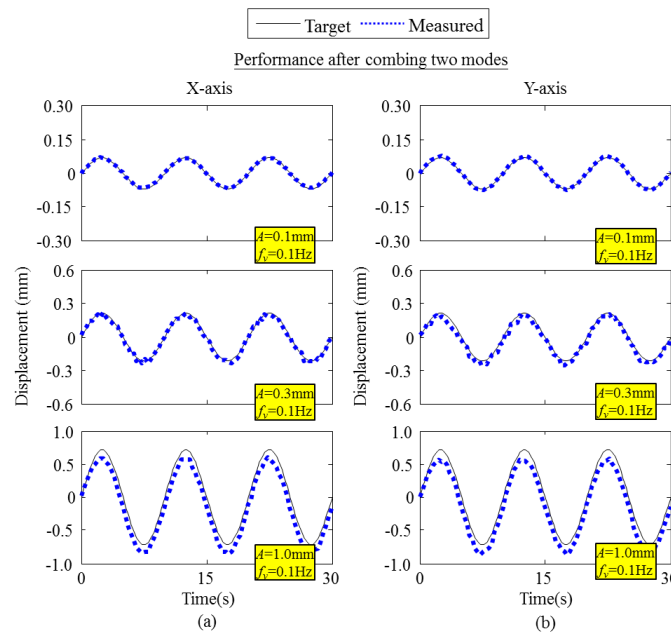

Fig. 19 Performance of the crack sensor for 2D sinusoidal motions after combing two modes under fixed f_v = 0.1 Hz: response along (a) X-axis and (b) Y-axis

To investigate the performance of sensor for tracking long-term crack propagation, a crack propagation time history of a distressed house due to environmental effect (Dowding and McKenna 2005) was programmed into the shake table under the setup of Fig. 5(b). The crack displacement ranged between -50 and 40 μm over a period of 54 hours. The sensor was set to run at the frame capture mode with one sample per hour. Results from the sensor were obtained and plotted in Fig. 22. It is seen that the proposed crack sensor is able to track this long-term crack propagation with reasonable accuracy and the discrepancy between the sensor output and the target profile is about 5 μm.
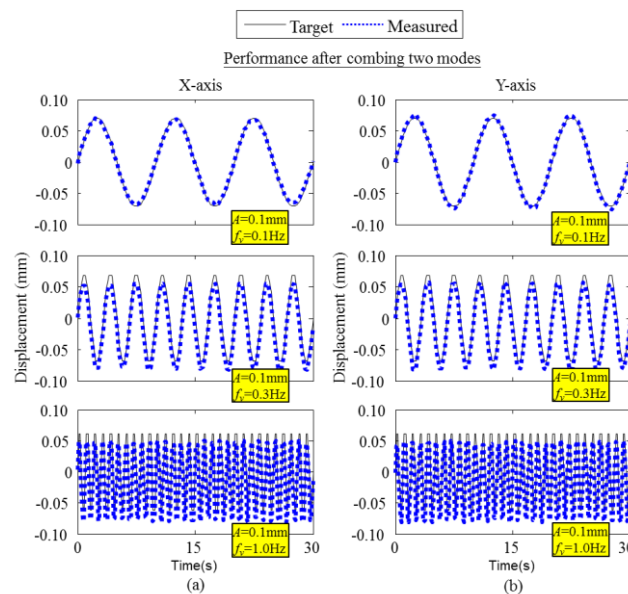

Fig. 20 Performance of the crack sensor for 2D sinusoidal motions after combing two modes under fixed A = 0.1 mm: response along (a) X-axis and (b) Y-axis
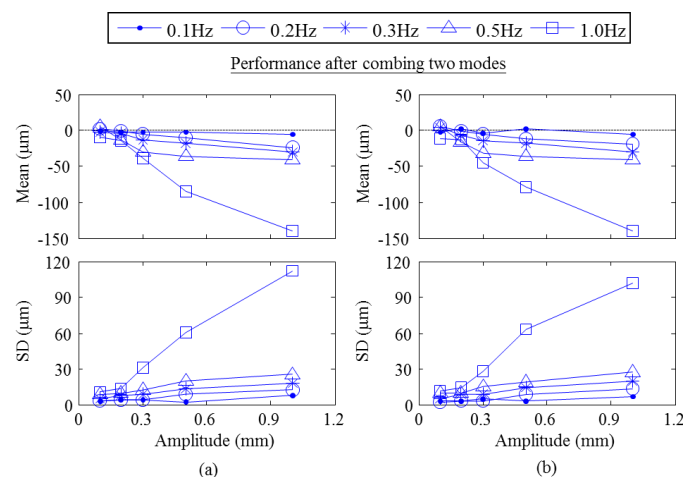

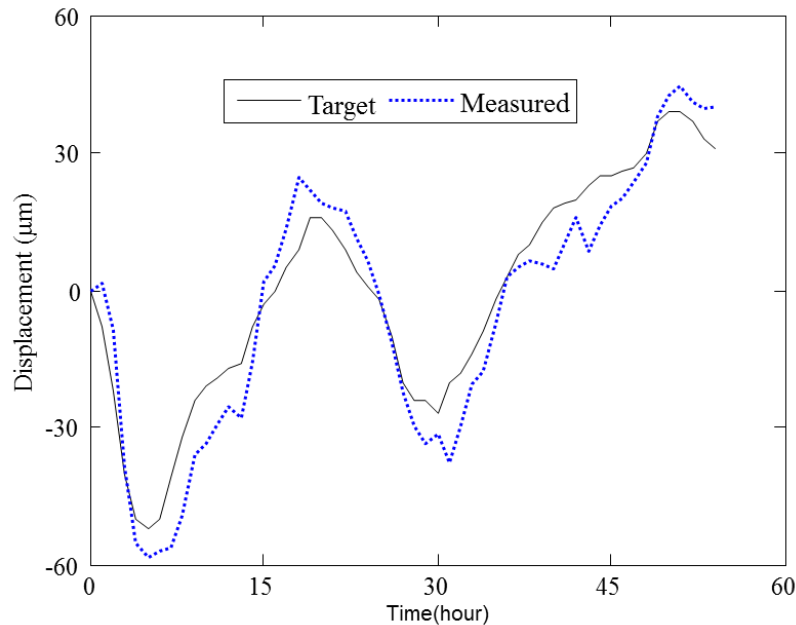Fig. 21 Means and SDs of measurement errors for 2D sinusoidal motions after combing two modes

Fig. 22 Performance of crack sensors for long-term crack propagation monitoring

6. Conclusions

Sensors and sensing systems are a new broad-based and technology-driven research area of increasingly emerging importance. In this paper, the specification and the design of a new wireless 2D crack sensor based on laser-based optical navigation technology were presented. This sensor was developed by incorporating a laser-based optical navigation sensor board (ADNS-9500) into a smart wireless platform (Imote2). To measure crack propagation, the Imote2 sent a signal to the ADNS-9500 to switch on the built-in laser and camera and collect a sequence of images reflected from the concrete surface. These acquired images could be processed in the ADNS-9500 directly (the navigation mode) or be sent to and processed in the Imote2 (the frame capture mode). The computed crack movement could then be wirelessly sent to a nearby computer. The design and the construction of this sensor were reported herein followed by some calibration tests on one prototype sensor. Test results showed that the sensor could offer sub millimeter accuracy under sinusoidal and step movement. The sensor's accuracy however was affected by the amplitude as well as the frequency of crack movement. It was seen that the two modes of operation offer complementary performance: the navigation mode was more accurate in tracking large amplitude and fast crack movement while the frame capture mode was more accurate for small and slow crack movement. Logical calculi based on the measured speed of movement were proposed to switch between the two modes. A set of sinusoidal tests were conducted to demonstrate the effectiveness of operating the sensor in combined modes. The sensor was further tested on a set of real measurement data to show the feasibility for monitoring long-term crack propagation. These results confirmed the applicability of such a crack sensor in actual implementation.

Acknowledgments

References

Avago Technologies, Inc. (2013a), Optical Mice and How They Work, http://www.avagotech.com/docs/AV02-1648EN (accessed on 10 June 2013).

Avago Technologies, Inc. (2013b), ADNS-9500 datasheet, http://www.avagotech.com/docs/AV02-1726EN (accessed on 10 June 2013).

BS8007 (1987), *Code of practice for design of concrete structures for retaining aqueous liquids.*

BS8110 (1997), *Structural use of concrete: Code of practice for design and construction.*

Cho, S., Jo, H., Jang, S., Park, J., Jung, H.J., Yun, C.B., Spencer, Jr. B.F. and Seo, J.W. (2010), "Structural health monitoring of a cable stayed bridge using smart sensor technology: data analysis", *Smart Struct. Syst.*, **6**(5-6), 439-459.

Ciliberto, C., Pattacini, U., Natale, L. Nori, F. and Metta, G. (2011), "Reexamining Lucas-Kanade method for real-time independent motion detection: Application to the iCub Humanoid robot", *Proceedings of the 2011 IEEE/RSJ International Conference on Intelligent Robots and Systems (IROS)*, San Francisco, Ca, USA, 25-30 Sept.

Crossbow Technology, Inc. (2013), Intel Imote2 Engineering Data Sheet, http://wsn.cse.wustl.edu/images/c/cb/Imote2-ds-rev2_2pdf. (accessed on 10 June 2013).

Dowding, C.H. and McKenna, L.M. (2005), "Crack response to long-term environmental and blast vibration effects", *J. Geotech. Geoenviron.*, **131**(9), 1151-1161.

Fairchild Semiconductor (2014), "MM74HC244 datasheet", http://pdf1.alldatasheet.com/datasheet-pdf/view/53758/FAIRCHILD/MM74HC244N.html (accessed on 17 March 2014).

Goodman, J.W. and Parry, G. (1984), *Laser Speckle and Related Phenomena*, Springer, New York.

Hyun, D., Yang, H.S., Park, H.R. and Park, J.S. (2009), "Differential optical navigation sensor for mobile robots", *Sensors Actuat. A: Physical*, 156(2), 296-301.

Jain, R., Kasturi, R., and Schunck, B.G. (1995), *Machine Vision*, McGraw-Hill, New York.

Jang, S., Jo, H., Cho, S., Mechitov, K., Rice, J.A., Sim, S.H., Jung, H.J., Yun, C.B., Spencer, Jr. B.F. and Agha, G. (2010), "Structural health monitoring of a cable-stayed bridge using smart sensor technology: deployment and evaluation", *Smart Struct. Syst.*, **6**(5-6), 439-459.

Ji, Y.F. and Chang, C.C. (2008), "Nontarget stereo vision technique for spatiotemporal response measurement of line-like structures", *J. Eng. Mech. - ASCE.*, **134**(6), 466-474.

Kotowsky, M.P. (2010), *Wireless Sensor Networks for Monitoring Cracks in Structures*, Master's thesis, Northwestern University, Evanston, Illinois.

Liao, C.M., Huang, P.S., Hwang, Y.Y., Chen, M. and Chiu, C.C. (2009), "Robust technique of analyzing and locating laser speckle patterns for optical computer mice", *Opt. Laser Eng.*, **47**(7-8), 875-883.

Lion Precision (2013), *Eddy-Current Sensors Overview*, http://www.lionprecision.com/index.php. (accessed on 10 June 2013).

Lucas, B.D. and Kanade, T. (1981), "An iterative image registration technique with an application to stereo vision", *Proceedings of the 7th Int. Joint Conf. on Artificial Intelligence* (IJCAI).

Maxim Integrated Products (2014), MAX3323EEPE datasheet, http://datasheets.maximintegrated.com/en/ds/MAX3322E-MAX3323E.pdf (accessed on 17 March 2014).

Measurement Specialties Inc. (2013), *Principles of the LVDT*, http://www.meas-spec.com. (accessed on 10 June 2013).

National Instruments (2013), *String Potentiometer and String Encoder Engineering Guide*, http://www.ni.com/. (accessed on 10 June 2013)

Park, K.W., Jeong, J.S., Min, K.J., Kim, Hwang, B.W. and Choi, W.T. (2007), Method for processing image

data of optical mouse, *US Patent 7212685 B2*.

Rice, J.A., Mechitov, K., Sim, S.H., Nagayama, T., Jang, S., Kim, R., Spencer Jr., B.F., Agha, G. and Fujino, Y. (2010), "Flexible smart sensor framework for autonomous structural health monitoring", *Smart Struct. Syst.*, **6**(5-6), 423-438.

Sim, S.H., Carbonell-Márquez, J.F., Spencer Jr., B.F. and Jo, H. (2010), "Decentralized random decrement technique for efficient data aggregation and system identification in wireless smart sensor networks", *Probabilist. Eng.Mech.*, **26**(1), 81-91.

Shang, Y. and Palmer, P.L. (2010), "Lunar lander's three-dimensional translation and yaw rotation motion estimation during a descent phase using optical navigation", *Acta Astronaut.*, **68**(1-2), 149-159.

Szeliski, R. (2011), *Computer Vision: Algorithms and Applications*, Springer.

BS